Chinese Journal of Aeronautics, (2019), 32(4): 906–920

Chinese Society of Aeronautics and Astronautics
& Beihang University

Chinese Journal of Aeronautics

cja@buaa.edu.cn
www.sciencedirect.com

Non-polynomial Zig-Zag and ESL shear deformation theory to study advanced composites

J.L. MANTARI [a,b,*], I.A. RAMOS [a], J.C. MONGE [c]

[a] *Faculty of Mechanical Engineering, Instituto de investigación en ingeniería naval (IDIIN), National University of Engineering (UNI), Lima 15333, Peru*
[b] *Department of Mechanical Engineering, University of New Mexico, Albuquerque, NM 87131, USA*
[c] *Faculty of Mechanical Engineering, Universidad de Ingeniería y Tecnología (UTEC), Lima 15063, Peru*

Received 19 August 2016; revised 25 May 2017; accepted 3 May 2018
Available online 15 February 2019

KEYWORDS

Analytical solution;
Composite materials;
CUF;
ESL;
Plate;
Trigonometric functions;
Zig-Zag effects

Abstract The mechanical behavior of advanced composites can be modeled mathematically through unknown variables and Shear Strain Thickness Functions (SSTFs). Such SSTFs can be of polynomial or non-polynomial nature and some parameters of non-polynomial SSTFs can be optimized to get optimal results. In this paper, these parameters are called "*r*" and "*s*" and they are the argument of the trigonometric SSTFs introduced within the Carrera Unified Formulation (CUF). The Equivalent Single Layer (ESL) governing equations are obtained by employing the Principle of Virtual Displacement (PVD) and are solved using Navier method solution. Furthermore, trigonometric expansion with Murakami theory was implemented in order to reproduce the Zig-Zag effects which are important for multilayer structures. Several combinations of optimization parameters are evaluated and selected by different criteria of average error. Results of the present unified trigonometrical theory with CUF bases confirm that it is possible to improve the stress and displacement results through the thickness distribution of models with reduced unknown variables. Since the idea is to find a theory with reduced numbers of unknowns, the present method appears to be an appropriate technique to select a simple model. However these optimization parameters depend on the plate geometry and the order of expansion or unknown variables. So, the topic deserves further research.

1. Introduction

Laminated composite materials are utilized in several areas, such as marine, aerospace, civil, biomedical and other industries. Their good mechanical properties (high specific stiffness, excellent fatigue strength, resistance to corrosion, etc.) have been the reason for an increase in demand and consequently the substitutes of traditional engineering materials such as

* Corresponding author.
E-mail address: josemantari@gmail.com (J.L. MANTARI).

Peer review under responsibility of Editorial Committee of CJA.

ELSEVIER Production and hosting by Elsevier

https://doi.org/10.1016/j.cja.2019.02.001

Nomenclature

CPT	Classical Plate Theory
CUF	Carrera Unified Formulation
ESL	Equivalent Single Layer
FSDT	First-order Shear Deformation Theory
GUF	Generalized Unified Formulation
HSDTs	Higher-order Shear Deformation Theories
LW	Layerwise
PVD	Principle of Virtual Displacement
SSDT	Sinusoidal Shear Deformation Theory
SSTFs	Shear Strain Thickness Functions

steel, aluminum, concrete, etc. Therefore, in order to understand the behavior of composite structures under different kinds of loads and boundary conditions, several theoretical and experimental studies were performed.

Classical Plate Theory (CPT) for metallic structures based on the Kirchhoff's assumptions, which neglects the shear deformation, was extended to laminated plates in order to study thin plates. First-order Shear Deformation Theory (FSDT) based on Reissner[1] and Mindlin[2] was introduced considering deformations in the section. A shear correction factor is used to correct the constant transverse shear strain component obtained with this theory. However, correction factor values depend on the material coefficients, geometry, boundary conditions and loading conditions, which are difficult to calculate. Therefore, Higher-order Shear Deformation Theories (HSDTs) were developed in order to overcome the limitation of FSDT.

The HSDTs can be developed using polynomial Shear Strain Thickness Functions (SSTFs), which can be seen from, for example, the articles by Reddy and Liu[3], Reddy[4], Levinson[5] and Librescu[6]. Further, non-polynomial shape functions were developed by Levy[7], Stein[8], Touratier[9], Soldatos[10], Karama[11], Mantari and Guedes Soares[12], Zenkour[13–16] and Mantari et al.[17–20]. An optimization of a HSDT based on trigonometric function for the bending analysis of functionally graded shells was proposed by Mantari and Guedes Soares[21], where parameters "*r*" and "*s*" were introduced in the displacement field in order to produce results close to 3D elasticity solutions.

Several investigators developed HSDTs to study advanced composites. Houari et al.[22] presented a new simple higher-order theory with only three unknowns considering sinusoidal thickness function on the transverse shear stress for solving bending and free vibration problems. Belabed et al.[23] proposed a higher-order theory with 5 unknowns which considered the stretching effect based on hyperbolic shear strain shape functions. Belkorissat et al.[24] developed a new nonlocal hyperbolic model to study free vibration of functionally graded nano plates based on Mori-Tanaka scheme. Boukhari et al.[25] proposed a deformation theory for wave propagation of an infinite functionally graded plates in the presence of thermal environment. Bennoun et al.[26] presented five unknown variables based on a hyperbolic expansion to study functionally graded sandwich plates. Bourada et al.[27] studied a refined trigonometric higher-order beam theory with three unknown variables for the bending and free vibration of functionally graded beams. Mahi et al.[28] calculated the free vibration for functionally graded plates using orthogonal polynomials associated with Ritz method. Tounsi et al.[29] presented a new HSDT of three unknown variables for the study of buckling and free vibration of sandwich functionally graded plates. Ait Yahia et al.[30] presented an interesting approximate model for functionally graded plates with porosity phases to study the wave propagation of plates. In fact, this paper can be used as a reference for ultrasonic inspection techniques and structural health monitoring. Hebali et al.[31] improved the plate theory proposed by El Meiche et al.[32] by studying the effect of considering nonzero transverse normal strain. Draiche et al.[33] studied a sinusoidal higher-order deformation theory for studying the flexure of angle and cross ply laminated composite plates.

Carrera Unified Formulation (CUF) was developed for composite laminated plates and shells[34–36] using originally Taylor's expansions of *N*-order. A Sinusoidal Shear Deformation Theory (SSDT) within the CUF framework was developed by Ferreira et al.[37] for static and free vibration analysis of laminated shells. Additionally, Generalized Unified Formulation (GUF), presented as a more general approach of CUF, was introduced for the first time by Demasi[38] for a single isotropic plate and extended for multilayered composite plate in Refs.[39–43]. Several non-polynomial expansions were developed by Filippi et al.[44] and Mantari et al.[45]. Furthermore, trigonometric expansion for laminated plate subject to thermal load was developed by Ramos et al.[46]. In order to obtain HSDTs with low computational cost, asymptotic/axiomatic technique was developed by Miglioretti et al.[47,48] and Carrera and Petrolo[49,50], where the effectiveness of each term of the displacement field is evaluated by means of elimination and comparison to a reference solution. The genetic algorithm to evaluate the importance of each displacement variable for finite element plate models was developed by Carrera and Miglioretti[51].

The present work uses an optimized method[52,53] based on two different optimized parameters which are "*r*" and "*s*" that are related to the in-plane and transverse displacement, respectively. The described parameters are contained in the argument

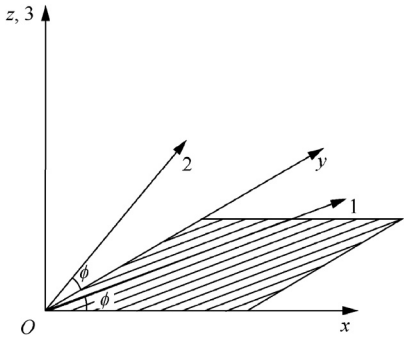

Fig. 1 Material coordinate (1, 2, 3) and plate coordinate (*x*, *y*, *z*).

Table 1 Comparison between exact, LD4 and ED4 solution.

Theory	$\bar{w}(z=h/4)$	Error (%)	$\bar{\sigma}_{xz}(z=h/4)$	Error (%)	$\bar{\sigma}_{zz}(z=h/4)$	Error (%)
Exact 3D (Ref.[43])	2.08755		0.09414		0.79428	
LD4	2.08744	0.005	0.09424	0.106	0.80154	0.914
ED4	2.03893	2.329	0.07634	18.908	0.13556	82.933

of trigonometric SSTFs in order to solve the analytical static problem of laminated plate by means of a compact formulation. Trigonometric expansion with Equivalent Single Layer (ESL) and Zig-Zag (Murakami) approach was introduced by using the Principle of Virtual Displacement (PVD) to obtain the unified governing equations, which are solved by employing Navier method solution. Several combinations of optimization parameters are evaluated and selected by different criteria of average error. Improvement in the deflection and stresses results for low-order expansion are presented for especial values of the parameters ("r" and "s") obtained by particular criteria of average error. However the optimization parameters depend on the plate geometry and the order of expansion of the utilized displacement field.

Table 2 Average errors with their respective weight.

Average error	w_1	w_2	w_3
Av1 $(\mathrm{err}\,\bar{w})$	1	0	0
Av2 $(\mathrm{err}\bar{\sigma}_{xx})$	0	1	0
Av3 $(\mathrm{err}\bar{\sigma}_{xz})$	0	0	1
Av4	1	1	1
Av5	3	2	1

2. Analytical modeling

2.1. Model kinematics

The through-the-plate-thickness unified displacement field developed by Carrera[34] for any order of expansion is expressed as follows:

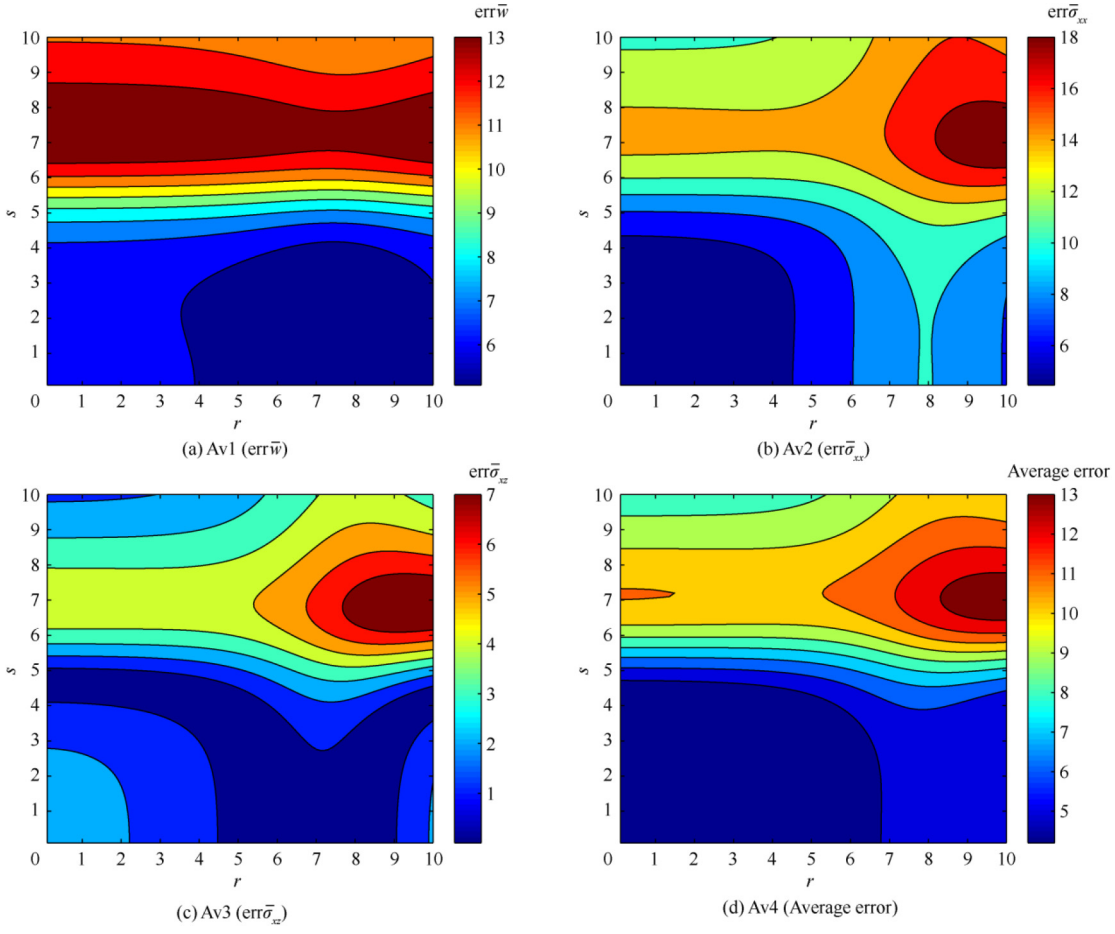

Fig. 2 Variation of percent errors for sin displacement as a function of parameters r and s $(N=2, a/h=4)$.

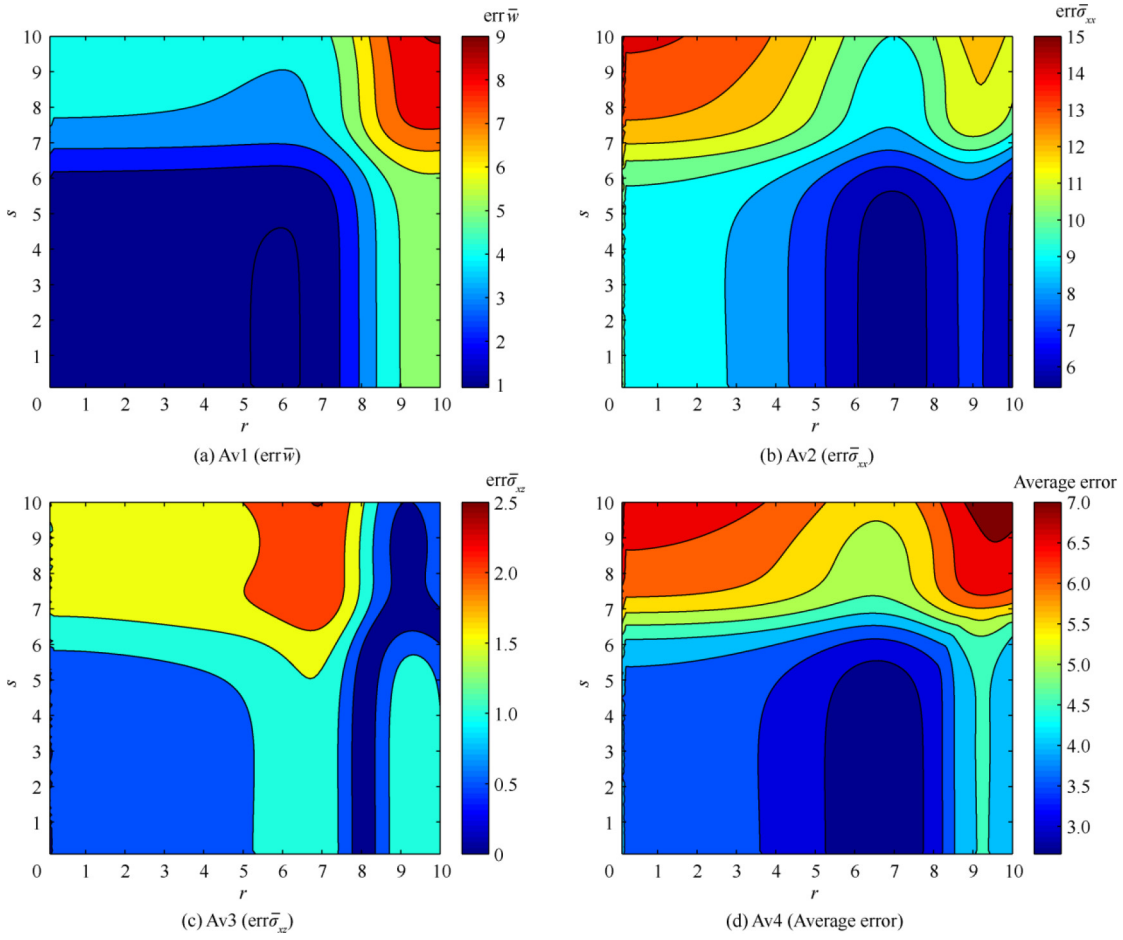

Fig. 3 Variation of percent errors for sin displacement as a function of parameters r and s ($N = 5, a/h = 4$).

$$\begin{cases} u_x = F_0 u_{x_0} + F_1 u_{x_1} + F_2 u_{x_2} + ... + F_N u_{x_N} \\ u_y = G_0 u_{y_0} + G_1 u_{y_1} + G_2 u_{y_2} + ... + G_N u_{y_N} \\ u_z = H_0 u_{z_0} + H_1 u_{z_1} + H_2 u_{z_2} + ... + H_N u_{z_N} \end{cases} \tag{1}$$

where F_N, G_N and H_N are functions through the thickness and N is the order of expansion. These equations can be grouped as follows:

$$\boldsymbol{u} = \begin{bmatrix} F_0 & 0 & 0 \\ 0 & G_0 & 0 \\ 0 & 0 & H_0 \end{bmatrix} \begin{bmatrix} u_{x_0} \\ u_{y_0} \\ u_{z_0} \end{bmatrix} + \begin{bmatrix} F_1 & 0 & 0 \\ 0 & G_1 & 0 \\ 0 & 0 & H_1 \end{bmatrix} \begin{bmatrix} u_{x_1} \\ u_{y_1} \\ u_{z_1} \end{bmatrix} + \begin{bmatrix} F_2 & 0 & 0 \\ 0 & G_2 & 0 \\ 0 & 0 & H_2 \end{bmatrix} \begin{bmatrix} u_{x_2} \\ u_{y_2} \\ u_{z_2} \end{bmatrix} + ... + \begin{bmatrix} F_N & 0 & 0 \\ 0 & G_N & 0 \\ 0 & 0 & H_N \end{bmatrix} \begin{bmatrix} u_{x_N} \\ u_{y_N} \\ u_{z_N} \end{bmatrix} \tag{2}$$

and in compact form:

$$\boldsymbol{u}_{(x,y,z)} = \boldsymbol{F}_\tau \boldsymbol{u}_\tau \quad \tau = 0, 1, 2, ..., N \tag{3}$$

where the subscript indicates summation according Einstein notation. F_τ and u_τ are given as

$$\boldsymbol{F}_\tau = \begin{bmatrix} F_\tau & 0 & 0 \\ 0 & G_\tau & 0 \\ 0 & 0 & H_\tau \end{bmatrix}, \quad \boldsymbol{u}_\tau = \begin{bmatrix} u_{x_\tau} \\ u_{y_\tau} \\ u_{z_\tau} \end{bmatrix} \tag{4}$$

This paper studies an axiomatic compact theory with Zig-Zag effect by exploring trigonometrical shear strain shape function (see Refs.[8–10] for single and Ref.[54] for multilayered plates) in a systematic manner. The results are compared with polynomial axiomatic expansions.

Polynomial, trigonometric, hyperbolic, exponential functions and different combinations of them are studied for beam in Ref.[55] and for plates in Refs.[44,45] within CUF framework. In the present work, optimized trigonometric functions have been implemented and compared with the classical Taylor expansion.

Trigonometric expansion (sin) developed in Ref.[46] is modified as follows:

$$\begin{cases} u_x = u_{x_0} + z u_{x_1} + \cos\left(\frac{rz}{h}\right) u_{x_2} + \sin\left(\frac{rz}{h}\right) u_{x_3} \\ \quad + \cos\left(\frac{2rz}{h}\right) u_{x_4} + \sin\left(\frac{2rz}{h}\right) u_{x_5} \\ u_y = u_{y_0} + z u_{y_1} + \cos\left(\frac{rz}{h}\right) u_{y_2} + \sin\left(\frac{rz}{h}\right) u_{y_3} + \cos\left(\frac{2rz}{h}\right) u_{y_4} \\ \quad + \sin\left(\frac{2rz}{h}\right) u_{y_5} \\ u_z = u_{z_0} + z u_{z_1} + \cos\left(\frac{sz}{h}\right) u_{z_2} + \sin\left(\frac{sz}{h}\right) u_{z_3} + \cos\left(\frac{2sz}{h}\right) u_{z_4} \\ \quad + \sinh\left(\frac{2sz}{h}\right) u_{z_5} \end{cases} \tag{5}$$

In order to reduce the number of optimized parameters, only 2 optimization parameters ("r" and "s") are included in the trigonometric SSTFs, where the parameter "r" is related to in-plane deformation (x and y directions) and the parameter

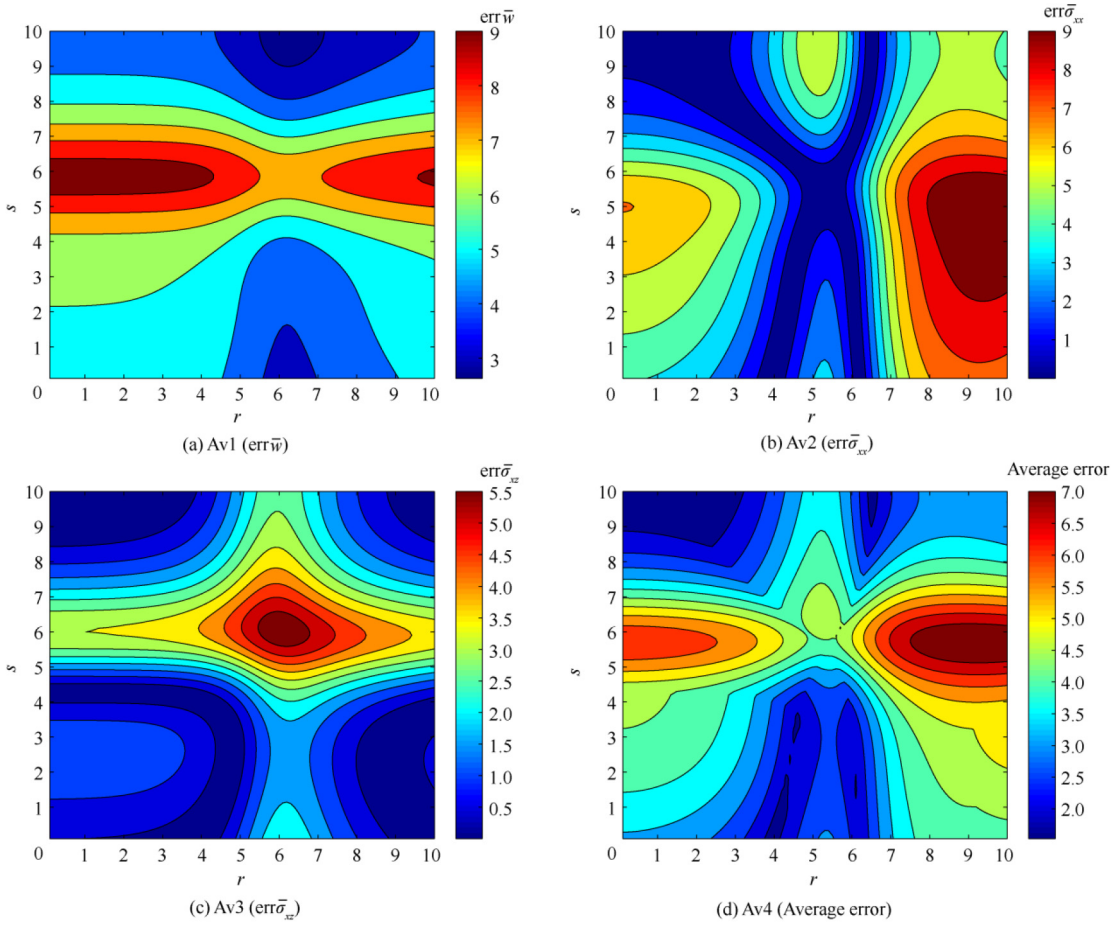

Fig. 4 Variation of percent errors for sin$Z$ displacement as a function of parameters r and s $(N = 2, a/h = 4)$.

"s" to the transverse deformation, i.e. thickness direction (z direction). The selection of these parameters within the SSTF was carried out with the idea to obtain close to 3D solution.

Additionally, the Mukarami Zig-Zag function is implemented in the trigonometric displacement field (sin Z).

$$\begin{cases} u_x = u_{x_0} + zu_{x_1} + \cos\left(\frac{rz}{h}\right)u_{x_2} + \sin\left(\frac{rz}{h}\right)u_{x_3} + \cos\left(\frac{2rz}{h}\right)u_{x_4} \\ \qquad +\sin\left(\frac{2rz}{h}\right)u_{x_5} + (-1)^k\zeta_k u_{x_6} \\ u_y = u_{y_0} + zu_{y_1} + \cos\left(\frac{rz}{h}\right)u_{y_2} + \sin\left(\frac{rz}{h}\right)u_{y_3} + \cos\left(\frac{2rz}{h}\right)u_{y_4} \\ \qquad +\sin\left(\frac{2rz}{h}\right)u_{y_5} + (-1)^k\zeta_k u_{y_6} \\ u_z = u_{z_0} + zu_{z_1} + \cos\left(\frac{sz}{h}\right)u_{z_2} + \sin\left(\frac{sz}{h}\right)u_{z_3} + \cos\left(\frac{2sz}{h}\right)u_{z_4} \\ \qquad +\sinh\left(\frac{2sz}{h}\right)u_{z_5} + (-1)^k\zeta_k u_{z_6} \end{cases} \tag{6}$$

where $(-1)^k\zeta_k$ is the Mukarami Zig-Zag function.

2.2. Elastic stress-strain relations

The stress $\boldsymbol{\sigma}^k$ and $\boldsymbol{\varepsilon}^k$ vectors of the kth layer are grouped according to CUF:

$$\begin{cases} \boldsymbol{\sigma}_p^k = \begin{bmatrix} \sigma_{xx}^k & \sigma_{yy}^k & \sigma_{xy}^k \end{bmatrix}^{\mathrm{T}} \\ \boldsymbol{\sigma}_n^k = \begin{bmatrix} \sigma_{xz}^k & \sigma_{yz}^k & \sigma_{zz}^k \end{bmatrix}^{\mathrm{T}} \\ \boldsymbol{\varepsilon}_p^k = \begin{bmatrix} \varepsilon_{xx}^k & \varepsilon_{yy}^k & \varepsilon_{xy}^k \end{bmatrix}^{\mathrm{T}} \\ \boldsymbol{\varepsilon}_n^k = \begin{bmatrix} \varepsilon_{xz}^k & \varepsilon_{yz}^k & \varepsilon_{zz}^k \end{bmatrix}^{\mathrm{T}} \end{cases} \tag{7}$$

where the subscript n is related to the in-plane components, while p to the out-of-plane components, and the strain-displacement relationships are given as

$$\begin{cases} \boldsymbol{\varepsilon}_p^k = \boldsymbol{D}_p\boldsymbol{u}^k \\ \boldsymbol{\varepsilon}_n^k = \boldsymbol{D}_n\boldsymbol{u}^k = \left(\boldsymbol{D}_{np} + \boldsymbol{D}_{nz}\right)\boldsymbol{u}^k \\ \boldsymbol{D}_p = \begin{bmatrix} \frac{\partial}{\partial x} & 0 & 0 \\ 0 & \frac{\partial}{\partial y} & 0 \\ \frac{\partial}{\partial y} & \frac{\partial}{\partial x} & 0 \end{bmatrix} \\ \boldsymbol{D}_{np} = \begin{bmatrix} 0 & 0 & \frac{\partial}{\partial x} \\ 0 & 0 & \frac{\partial}{\partial y} \\ 0 & 0 & 0 \end{bmatrix}, \ \boldsymbol{D}_{nz} = \begin{bmatrix} \frac{\partial}{\partial z} & 0 & 0 \\ 0 & \frac{\partial}{\partial z} & 0 \\ 0 & 0 & \frac{\partial}{\partial z} \end{bmatrix} \end{cases} \tag{8}$$

The stress-strain relationships in the material coordinates (see Fig. 1) of the kth layer can be expressed as

$$\begin{bmatrix} \sigma_{11}^k \\ \sigma_{22}^k \\ \sigma_{12}^k \\ \sigma_{13}^k \\ \sigma_{23}^k \\ \sigma_{33}^k \end{bmatrix} = \begin{bmatrix} C_{11}^k & C_{12}^k & 0 & 0 & 0 & C_{13}^k \\ C_{12}^k & C_{22}^k & 0 & 0 & 0 & C_{23}^k \\ 0 & 0 & C_{66}^k & 0 & 0 & 0 \\ 0 & 0 & 0 & C_{55}^k & 0 & 0 \\ 0 & 0 & 0 & 0 & C_{44}^k & 0 \\ C_{13}^k & C_{23}^k & 0 & 0 & 0 & C_{33}^k \end{bmatrix} \begin{bmatrix} \varepsilon_{11}^k \\ \varepsilon_{22}^k \\ \varepsilon_{12}^k \\ \varepsilon_{13}^k \\ \varepsilon_{23}^k \\ \varepsilon_{33}^k \end{bmatrix} \tag{9}$$

where stiffness coefficient C_{ij}^k are given below for an orthotropic material:

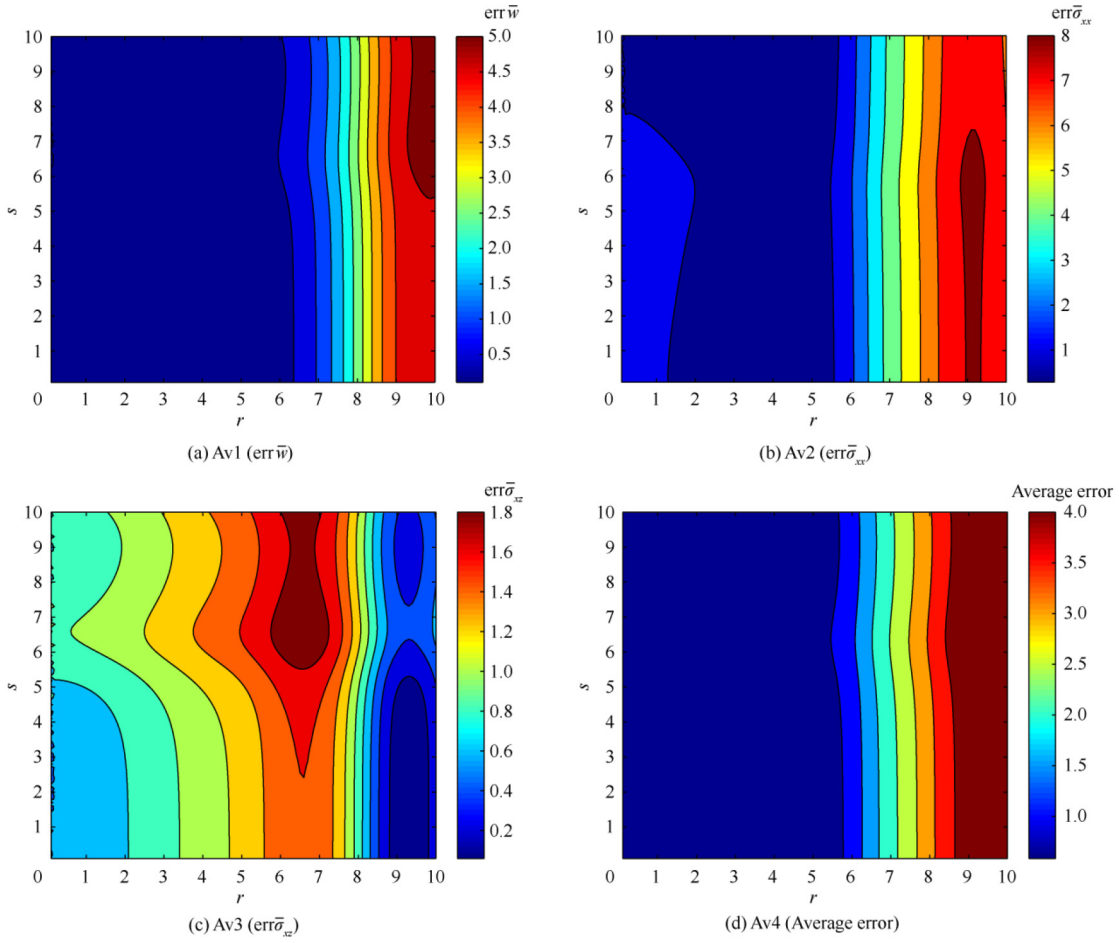

Fig. 5 Variation of percent errors for sin$Z$ displacement as a function of parameters r and s $(N = 5, a/h = 4)$.

$$\begin{cases} C_{11}^k = E_1^k \frac{1-\upsilon_{23}^k \upsilon_{32}^k}{\Delta}, C_{12}^k = E_2^k \frac{\upsilon_{12}^k + \upsilon_{32}^k \upsilon_{13}^k}{\Delta}, C_{44}^k = G_{23}^k \\ C_{22}^k = E_2^k \frac{1-\upsilon_{13}^k \upsilon_{31}^k}{\Delta}, C_{13}^k = E_3^k \frac{\upsilon_{13}^k + \upsilon_{12}^k \upsilon_{23}^k}{\Delta}, C_{55}^k = G_{13}^k \\ C_{33}^k = E_3^k \frac{1-\upsilon_{12}^k \upsilon_{21}^k}{\Delta}, C_{23}^k = E_3^k \frac{\upsilon_{23}^k + \upsilon_{21}^k \upsilon_{13}^k}{\Delta}, C_{66}^k = G_{12}^k \end{cases} \tag{10}$$

and

$$\Delta = 1 - \upsilon_{12}^k \upsilon_{21}^k - \upsilon_{23}^k \upsilon_{32}^k - \upsilon_{31}^k \upsilon_{13}^k - 2\upsilon_{12}^k \upsilon_{32}^k \upsilon_{13}^k \tag{11}$$

According to Eq. (7), the material matrices can be grouped as

$$\begin{cases} \boldsymbol{\sigma}_p^k = \widetilde{\boldsymbol{C}}_{pp}^k \boldsymbol{\varepsilon}_p^k + \widetilde{\boldsymbol{C}}_{np}^k \boldsymbol{\varepsilon}_n^k \\ \boldsymbol{\sigma}_n^k = \widetilde{\boldsymbol{C}}_{np}^k \boldsymbol{\varepsilon}_p^k + \widetilde{\boldsymbol{C}}_{nn}^k \boldsymbol{\varepsilon}_n^k \end{cases} \tag{12}$$

where

$$\begin{cases} \widetilde{\boldsymbol{C}}_{pp}^k = \begin{bmatrix} \widetilde{C}_{11}^k & \widetilde{C}_{12}^k & 0 \\ \widetilde{C}_{12}^k & \widetilde{C}_{22}^k & 0 \\ 0 & 0 & \widetilde{C}_{66}^k \end{bmatrix}, \widetilde{\boldsymbol{C}}_{nn}^k = \begin{bmatrix} \widetilde{C}_{55}^k & 0 & 0 \\ 0 & \widetilde{C}_{44}^k & 0 \\ 0 & 0 & \widetilde{C}_{33}^k \end{bmatrix} \\ \widetilde{\boldsymbol{C}}_{np}^k = \begin{bmatrix} 0 & 0 & 0 \\ 0 & 0 & 0 \\ \widetilde{C}_{13}^k & \widetilde{C}_{23}^k & 0 \end{bmatrix}, \widetilde{\boldsymbol{C}}_{pn}^k = \begin{bmatrix} 0 & 0 & \widetilde{C}_{13}^k \\ 0 & 0 & \widetilde{C}_{23}^k \\ 0 & 0 & 0 \end{bmatrix} \end{cases} \tag{13}$$

where $\widetilde{C}_{ij}^k$ are elastic coefficients in the plate coordinates.

2.3. Principle of virtual work

Considering the static version of the principle of virtual works, the following expression holds:

$$\delta L_{\mathrm{i}}^k = \delta L_{\mathrm{e}}^k \tag{14}$$

where L_{e}^k is the external virtual works and L_{i}^k the strain energy. Develop the abode expression for the kth layer, and the following expressions can be obtained:

$$\sum_{k=1}^{N_{\mathrm{l}}} \int_{\Omega_k} \int_{A_k} \left\{ \left(\delta \boldsymbol{\varepsilon}_p^k\right)^{\mathrm{T}} \boldsymbol{\sigma}_p^k + \left(\delta \boldsymbol{\varepsilon}_n^k\right)^{\mathrm{T}} \boldsymbol{\sigma}_n^k \right\} \mathrm{d}\Omega_k \mathrm{d}z = \sum_{k=1}^{N_{\mathrm{l}}} \delta L_{\mathrm{e}}^k \tag{15}$$

where $\boldsymbol{\varepsilon}^k$ and $\boldsymbol{\sigma}^k$ are the strain and the stress vectors of the kth layer and N_{l} stands for number of layers.

Using Eqs. (3) and (8), the expression becomes

$$\begin{aligned} \delta L_{\mathrm{i}}^k = \int_{\Omega_k} \Big\{ & \left(\boldsymbol{D}_p \boldsymbol{F}_\tau \delta \boldsymbol{u}_\tau\right)^{\mathrm{T}} \left(F_s \boldsymbol{C}_{pp}^k \boldsymbol{D}_p \boldsymbol{u}_s + \boldsymbol{F}_s \boldsymbol{C}_{pn}^k \boldsymbol{D}_{np} \boldsymbol{u}_s + \boldsymbol{F}_{s_{,z}} \boldsymbol{C}_{pn}^k \boldsymbol{u}_s \right) \\ & + \left(\boldsymbol{D}_{np} \boldsymbol{F}_\tau \delta \boldsymbol{u}_\tau\right)^{\mathrm{T}} \left(\boldsymbol{F}_s \boldsymbol{C}_{np}^k \boldsymbol{D}_p \boldsymbol{u}_s + \boldsymbol{F}_s \boldsymbol{C}_{nn}^k \boldsymbol{D}_{np} \boldsymbol{u}_s + \boldsymbol{F}_{s_{,z}} \boldsymbol{C}_{nn}^k \boldsymbol{u}_s \right) \\ & + \left(\boldsymbol{F}_{\tau_{,z}} \delta \boldsymbol{u}_\tau\right)^{\mathrm{T}} \left(\boldsymbol{F}_s \boldsymbol{C}_{np}^k \boldsymbol{D}_p \boldsymbol{u}_s + \boldsymbol{F}_s \boldsymbol{C}_{nn}^k \boldsymbol{D}_{np} \boldsymbol{u}_s + \boldsymbol{F}_{s_{,z}} \boldsymbol{C}_{nn}^k \boldsymbol{u}_s \right) \Big\} \mathrm{d}\Omega_k \end{aligned} \tag{16}$$

The subscript z indicates partial derivation with respect to z. By applying integration by parts (see Eq. (17)) to Eq. (16)

Table 3 Non-dimensionless results for optimized trigonometric expansion (sin).

N	Theory	r	s	$\bar{w}(z=h/4)$	Av1 (%)	$\bar{\sigma}_{xx}(z=0)$	Av2 (%)	$\bar{\sigma}_{xz}(z=-h/4)$	Av3 (%)	Av4 (%)	Av5 (%)
	LD4			2.0874		0.5965		0.3172			
2	ED2			1.9567	6.26	0.5696	4.51	0.3243	2.24	4.34	5.01
	sin	1	1	1.9574	6.23	0.5694	4.54	0.3241	2.18	4.32	4.99
	sin-opt1	7.4	2	1.9814	5.08	0.538	9.81	0.3147	0.79	5.22	5.94
	sin-opt2	0.1	1.9	1.9578	6.21	0.5698	4.48	0.3241	2.18	4.29	4.96
	sin-opt3	4.1	4.2	1.9458	6.78	0.557	6.62	0.3172	0.00	4.47	5.60
	sin-opt4	4.5	2.8	1.965	5.86	0.5608	5.98	0.3196	0.76	4.20	5.05
	sin-opt5	0.1	2.3	1.9578	6.21	0.5698	4.48	0.3239	2.11	4.27	4.95
3	ED3			2.0312	2.69	0.5186	13.06	0.3235	1.99	5.91	6.03
	sin	1	1	2.031	2.70	0.5183	13.11	0.3234	1.95	5.92	6.05
	sin-opt1	0.1	0.1	2.0312	2.69	0.5186	13.06	0.3235	1.99	5.91	6.03
	sin-opt2	10	1.4	1.9668	5.78	0.5581	6.44	0.3209	1.17	4.46	5.23
	sin-opt3	0.5	8.5	1.9453	6.81	0.4869	18.37	0.3172	0.00	8.39	9.53
	sin-opt4	10	2.2	1.9673	5.75	0.5579	6.47	0.3208	1.13	4.45	5.22
	sin-opt5	10	2.1	1.9672	5.76	0.558	6.45	0.3208	1.13	4.45	5.22
4	ED4			2.0389	2.32	0.5087	14.72	0.3187	0.47	5.84	6.15
	sin	1	1	2.0383	2.35	0.5085	14.75	0.3188	0.50	5.87	6.18
	sin-opt1	0.1	0.4	2.0389	2.32	0.5087	14.72	0.3188	0.50	5.85	6.15
	sin-opt2	10	1.4	1.9685	5.70	0.5654	5.21	0.3205	1.04	3.98	4.76
	sin-opt3	5.6	8.9	1.9439	6.87	0.4861	18.51	0.3172	0.00	8.46	9.61
	sin-opt4	10	2.3	1.9684	5.70	0.5653	5.23	0.3204	1.01	3.98	4.76
	sin-opt5	10	1.9	1.9685	5.70	0.5654	5.21	0.3204	1.01	3.97	4.75
5	ED5			2.0618	1.23	0.5398	9.51	0.3151	0.66	3.80	3.89
	sin	1	1	2.062	1.22	0.5402	9.44	0.3151	0.66	3.77	3.86
	sin-opt1	6	1.3	2.0678	0.94	0.5602	6.09	0.3134	1.20	2.74	2.70
	sin-opt2	7	0.3	2.0592	1.35	0.5641	5.43	0.313	1.32	2.70	2.71
	sin-opt3	8.1	4.7	2.0159	3.43	0.5579	6.47	0.3172	0.00	3.30	3.87
	sin-opt4	6.6	2.1	2.0653	1.06	0.5634	5.55	0.3129	1.36	2.65	2.60
	sin-opt5	6.5	1.8	2.0661	1.02	0.563	5.62	0.3129	1.36	2.66	2.61

Note: The normal stress $\bar{\sigma}_{xx}$ is evaluated in the bottom layer.

$$\int_{\Omega_k}(\boldsymbol{D}_\Omega\delta\boldsymbol{a}_\tau)^{\mathrm{T}}\boldsymbol{a}_s\mathrm{d}\Omega_k=-\int_{\Omega_k}(\delta\boldsymbol{a}_\tau)^{\mathrm{T}}\left(\boldsymbol{D}_\Omega^{\mathrm{T}}\boldsymbol{a}_s\right)\mathrm{d}\Omega_k+\int_{\Omega_k}(\delta\boldsymbol{a}_\tau)^{\mathrm{T}}\left(\boldsymbol{I}_\Omega^{\Gamma}\boldsymbol{a}_s\right)\mathrm{d}\Gamma \tag{17}$$

the plate boundary and internal governing equations for the case problem are obtained:

$$\delta L_{\mathrm{i}}^k=\int_{\Omega_k}(\delta\boldsymbol{u}_\tau)^{\mathrm{T}}K_{uu}^{k\tau s}\boldsymbol{u}_s\mathrm{d}\Omega_k+\int_{\Gamma_k}(\delta\boldsymbol{u}_\tau)^{\mathrm{T}}\Pi_{uu}^{k\tau s}\boldsymbol{u}_s\mathrm{d}\Gamma_k \tag{18}$$

where $K_{uu}^{k\tau s}$ is the stiffness matrix in the form of fundamental nucleus and $\Pi_{uu}^{k\tau s}$ represent the boundary conditions. These terms are expressed as follows:

$$\begin{aligned}K_{uu}^{k\tau s}=&-\int_z\left(\boldsymbol{F}_\tau\boldsymbol{D}_p^{\mathrm{T}}\boldsymbol{C}_{pp}^k\boldsymbol{D}_p\boldsymbol{F}_s+\boldsymbol{F}_\tau\boldsymbol{D}_p^{\mathrm{T}}\boldsymbol{C}_{pn}^k\boldsymbol{D}_{np}\boldsymbol{F}_s+\boldsymbol{F}_\tau\boldsymbol{D}_p^{\mathrm{T}}\boldsymbol{C}_{pn}^k\boldsymbol{F}_{s_z}\right)\mathrm{d}z\\&-\int_z\left(\boldsymbol{F}_\tau\boldsymbol{D}_{np}^{\mathrm{T}}\boldsymbol{C}_{np}^k\boldsymbol{D}_p\boldsymbol{F}_s+\boldsymbol{F}_\tau\boldsymbol{D}_{np}^{\mathrm{T}}\boldsymbol{C}_{nn}^k\boldsymbol{D}_{np}\boldsymbol{F}_s+\boldsymbol{F}_\tau\boldsymbol{D}_{np}^{\mathrm{T}}\boldsymbol{C}_{nn}^k\boldsymbol{F}_{s_z}\right)\mathrm{d}z\\&+\int_z\left(\boldsymbol{F}_{\tau_z}\boldsymbol{C}_{np}^k\boldsymbol{D}_p\boldsymbol{F}_s+\boldsymbol{F}_{\tau_z}\boldsymbol{C}_{nn}^k\boldsymbol{D}_{np}\boldsymbol{F}_s+\boldsymbol{F}_{\tau_z}\boldsymbol{C}_{nn}^k\boldsymbol{F}_{s_z}\right)\mathrm{d}z\end{aligned} \tag{19}$$

$$\begin{aligned}\Pi_{uu}^{k\tau s}=&\int_z\left(\boldsymbol{F}_\tau\boldsymbol{I}_p^{\mathrm{T}}\boldsymbol{C}_{pp}^k\boldsymbol{D}_p\boldsymbol{F}_s+\boldsymbol{F}_\tau\boldsymbol{I}_p^{\mathrm{T}}\boldsymbol{C}_{pn}^k\boldsymbol{D}_{np}\boldsymbol{F}_s+\boldsymbol{F}_\tau\boldsymbol{I}_p^{\mathrm{T}}\boldsymbol{C}_{pn}^k\boldsymbol{F}_{s_z}\right)\mathrm{d}z\\&+\int_z\left(\boldsymbol{F}_\tau\boldsymbol{I}_{np}^{\mathrm{T}}\boldsymbol{C}_{np}^k\boldsymbol{D}_p\boldsymbol{F}_s+\boldsymbol{F}_\tau\boldsymbol{I}_{np}^{\mathrm{T}}\boldsymbol{C}_{nn}^k\boldsymbol{D}_{np}\boldsymbol{F}_s+\boldsymbol{F}_\tau\boldsymbol{I}_{np}^{\mathrm{T}}\boldsymbol{C}_{nn}^k\boldsymbol{F}_{s_z}\right)\mathrm{d}z\end{aligned} \tag{20}$$

$$\boldsymbol{I}_p=\begin{bmatrix}1&0&0\\0&1&0\\1&1&0\end{bmatrix},\ \boldsymbol{I}_{np}=\begin{bmatrix}0&0&1\\0&0&1\\0&0&0\end{bmatrix} \tag{21}$$

On the other hand, the external virtual work δL_{e}^k due to a load q_z applied on the top face ($z=h/2$) can be expressed in the following manner:

$$\delta L_{\mathrm{e}}^k=\int_{\Omega_k}(\delta\boldsymbol{u}_\tau)^{\mathrm{T}}\boldsymbol{P}_u^{k\tau s}\boldsymbol{u}_s\mathrm{d}\Omega_k \tag{22}$$

where

$$\boldsymbol{P}_u^{k\tau s}=\begin{bmatrix}0&0&q_zH_\tau(z=h/2)\end{bmatrix}^{\mathrm{T}} \tag{23}$$

Finally, the governing equations are

$$\left(\delta\boldsymbol{u}_\tau^k\right)^{\mathrm{T}}:K_{uu}^{k\tau s}\boldsymbol{u}_s^k=\boldsymbol{P}_u^{k\tau} \tag{24}$$

2.4. Analytical solution

Navier type closed form solution can be applied in simply supported plates. So, the displacement variable and the distributed load can be expressed in the following Fourier series:

Table 4 Non-dimensionless results for optimized trigonometric expansion (sin$Z$).

N	Theory	r	s	$\bar{w}(z=h/4)$	Av1 (%)	$\bar{\sigma}_{xx}(z=0)$	Av2 (%)	$\bar{\sigma}_{xz}(z=-h/4)$	Av3 (%)	Av4 (%)	Av5 (%)
	LD4			2.0874		0.5965		0.3172			
2	EDZ2			1.9623	5.99	0.564	5.45	0.3217	1.42	4.29	5.05
	sin$Z$	1	1	1.9661	5.81	0.5692	4.58	0.3201	0.91	3.77	4.58
	sin$Z$-opt1	6.2	10	2.0325	2.63	0.6082	1.96	0.3082	2.84	2.48	2.44
	sin$Z$-opt2	5.5	5.7	1.9213	7.96	0.5965	0.00	0.3005	5.26	4.41	4.86
	sin$Z$-opt3	9.9	10	2.0023	4.08	0.5666	5.01	0.3172	0.00	3.03	3.71
	sin$Z$-opt4	2	9.5	1.9923	4.56	0.5964	0.02	0.3173	0.03	1.53	2.29
	sin$Z$-opt5	6.5	10	2.0315	2.68	0.5969	0.07	0.309	2.59	1.78	1.79
3	EDZ3			2.0422	2.17	0.5556	6.86	0.3258	2.71	3.91	3.82
	sin$Z$	1	1	2.0492	1.83	0.5621	5.77	0.3247	2.36	3.32	3.23
	sin$Z$-opt1	2	9.9	2.0874	0.00	0.586	1.76	0.3248	2.40	1.39	0.99
	sin$Z$-opt2	3.3	8.8	2.0999	0.60	0.5965	0.00	0.3249	2.43	1.01	0.70
	sin$Z$-opt3	5.3	8.1	2.0982	0.52	0.5971	0.10	0.3172	0.00	0.21	0.29
	sin$Z$-opt4	5.1	7.8	2.0886	0.06	0.5961	0.07	0.3178	0.19	0.10	0.08
	sin$Z$-opt5	5.1	7.8	2.0886	0.06	0.5961	0.07	0.3178	0.19	0.10	0.08
4	EDZ4			2.0728	0.70	0.5813	2.55	0.3174	0.06	1.10	1.21
	sin$Z$	1	1	2.0701	0.83	0.5792	2.90	0.3177	0.16	1.30	1.41
	sin$Z$-opt1	0.1	0.1	2.0863	0.05	0.592	0.75	0.3155	0.54	0.45	0.37
	sin$Z$-opt2	1.7	0.1	2.0856	0.09	0.5922	0.72	0.3153	0.60	0.47	0.38
	sin$Z$-opt3	3.8	0.8	2.0695	0.86	0.5821	2.41	0.3172	0.00	1.09	1.23
	sin$Z$-opt4	0.1	0.1	2.0863	0.05	0.592	0.75	0.3155	0.54	0.45	0.37
	sin$Z$-opt5	0.1	0.1	2.0863	0.05	0.592	0.75	0.3155	0.54	0.45	0.37
5	EDZ5			2.0827	0.23	0.5901	1.07	0.3151	0.66	0.65	0.58
	sin$Z$	1	1	2.0829	0.22	0.5903	1.04	0.315	0.69	0.65	0.57
	sin$Z$-opt1	4.6	0.2	2.0852	0.11	0.5935	0.50	0.3134	1.20	0.60	0.42
	sin$Z$-opt2	4.5	10	2.0818	0.27	0.5948	0.28	0.3126	1.45	0.67	0.47
	sin$Z$-opt3	9.3	0.1	1.9877	4.78	0.5486	8.03	0.317	0.06	4.29	5.08
	sin$Z$-opt4	4.1	0.2	2.0851	0.11	0.5933	0.54	0.3137	1.10	0.58	0.42
	sin$Z$-opt5	4.4	0.2	2.0852	0.11	0.5935	0.50	0.3135	1.17	0.59	0.41

$$\begin{bmatrix} u_{x_s} \\ u_{y_s} \\ u_{z_s} \\ q_z \end{bmatrix} = \sum_{m,n} \begin{bmatrix} U_{x_s}\cos(\alpha x_k)\sin(\beta y_k) \\ U_{y_s}\sin(\alpha x_k)\cos(\beta y_k) \\ U_{z_s}\sin(\alpha x_k)\sin(\beta y_k) \\ Q_z\sin(\alpha x_k)\sin(\beta y_k) \end{bmatrix} \qquad 0 \leqslant x \leqslant a, 0 \leqslant y \leqslant b \tag{25}$$

where

$$\alpha = \frac{m\pi}{a},\ \beta = \frac{n\pi}{b} \tag{26}$$

Therefore, the governing equation becomes

$$\begin{bmatrix} \overset{-k\tau s}{K}_{uu11} & \overset{-k\tau s}{K}_{uu12} & \overset{-k\tau s}{K}_{uu13} \\ \overset{-k\tau s}{K}_{uu21} & \overset{-k\tau s}{K}_{uu22} & \overset{-k\tau s}{K}_{uu23} \\ \overset{-k\tau s}{K}_{uu31} & \overset{-k\tau s}{K}_{uu32} & \overset{-k\tau s}{K}_{uu33} \end{bmatrix} \begin{bmatrix} U^k_{x_s} \\ U^k_{y_s} \\ U^k_{z_s} \end{bmatrix} = \begin{bmatrix} 0 \\ 0 \\ \bar{H}_z Q_z \end{bmatrix} \tag{27}$$

where

$$\begin{cases} \overset{-k\tau s}{K}_{uu11} = \int_z \left(\widetilde{C}^k_{55} \boldsymbol{F}_{\tau,z} \boldsymbol{F}_{s,z} + \alpha^2 \widetilde{C}^k_{11} \boldsymbol{F}_\tau \boldsymbol{F}_s + \beta^2 \widetilde{C}^k_{66} \boldsymbol{F}_\tau \boldsymbol{F}_s \right) \mathrm{d}z \\ \overset{-k\tau s}{K}_{uu12} = \int_z \left(\alpha\beta \widetilde{C}^k_{12} \boldsymbol{F}_\tau \boldsymbol{G}_s + \alpha\beta \widetilde{C}^k_{66} \boldsymbol{F}_\tau \boldsymbol{G}_s \right) \mathrm{d}z \\ \overset{-k\tau s}{K}_{uu13} = \int_z \left(-\alpha \widetilde{C}^k_{13} \boldsymbol{F}_\tau \boldsymbol{H}_{s,z} + \alpha \widetilde{C}^k_{55} \boldsymbol{F}_{\tau,z} \boldsymbol{H}_s \right) \mathrm{d}z \\ \overset{-k\tau s}{K}_{uu21} = \int_z \left(\alpha\beta \widetilde{C}^k_{12} \boldsymbol{G}_\tau \boldsymbol{F}_s + \alpha\beta \widetilde{C}^k_{66} \boldsymbol{G}_\tau \boldsymbol{F}_s \right) \mathrm{d}z \\ \overset{-k\tau s}{K}_{uu22} = \int_z \left(\widetilde{C}^k_{44} \boldsymbol{G}_{\tau,z} \boldsymbol{G}_{s,z} + \alpha^2 \widetilde{C}^k_{66} \boldsymbol{G}_\tau \boldsymbol{G}_s + \beta^2 \widetilde{C}^k_{22} \boldsymbol{G}_\tau \boldsymbol{G}_s \right) \mathrm{d}z \\ \overset{-k\tau s}{K}_{uu23} = \int_z \left(-\beta \widetilde{C}^k_{23} \boldsymbol{G}_\tau \boldsymbol{H}_{s,z} + \beta \widetilde{C}^k_{44} \boldsymbol{G}_{\tau,z} \boldsymbol{H}_s \right) \mathrm{d}z \\ \overset{-k\tau s}{K}_{uu31} = \int_z \left(\alpha \widetilde{C}^k_{55} \boldsymbol{H}_\tau \boldsymbol{F}_{s,z} - \alpha \widetilde{C}^k_{13} \boldsymbol{H}_{\tau,z} \boldsymbol{F}_s \right) \mathrm{d}z \\ \overset{-k\tau s}{K}_{uu32} = \int_z \left(\beta \widetilde{C}^k_{44} \boldsymbol{H}_\tau \boldsymbol{G}_{s,z} - \beta \widetilde{C}^k_{23} \boldsymbol{H}_{\tau,z} \boldsymbol{G}_s \right) \mathrm{d}z \\ \overset{-k\tau s}{K}_{uu33} = \int_z \left(\widetilde{C}^k_{33} \boldsymbol{H}_{\tau,z} \boldsymbol{H}_{s,z} + \alpha^2 \widetilde{C}^k_{55} \boldsymbol{H}_\tau \boldsymbol{H}_s + \beta^2 \widetilde{C}^k_{44} \boldsymbol{H}_\tau \boldsymbol{H}_s \right) \mathrm{d}z \end{cases} \tag{28}$$

The explicit expressions of the fundamental stiffness nuclei, $\overset{-k\tau s}{K}_{uu}$, are unique for any combination of optimized parameter. In contrast to classical polynomial expansions, the exact Gauss

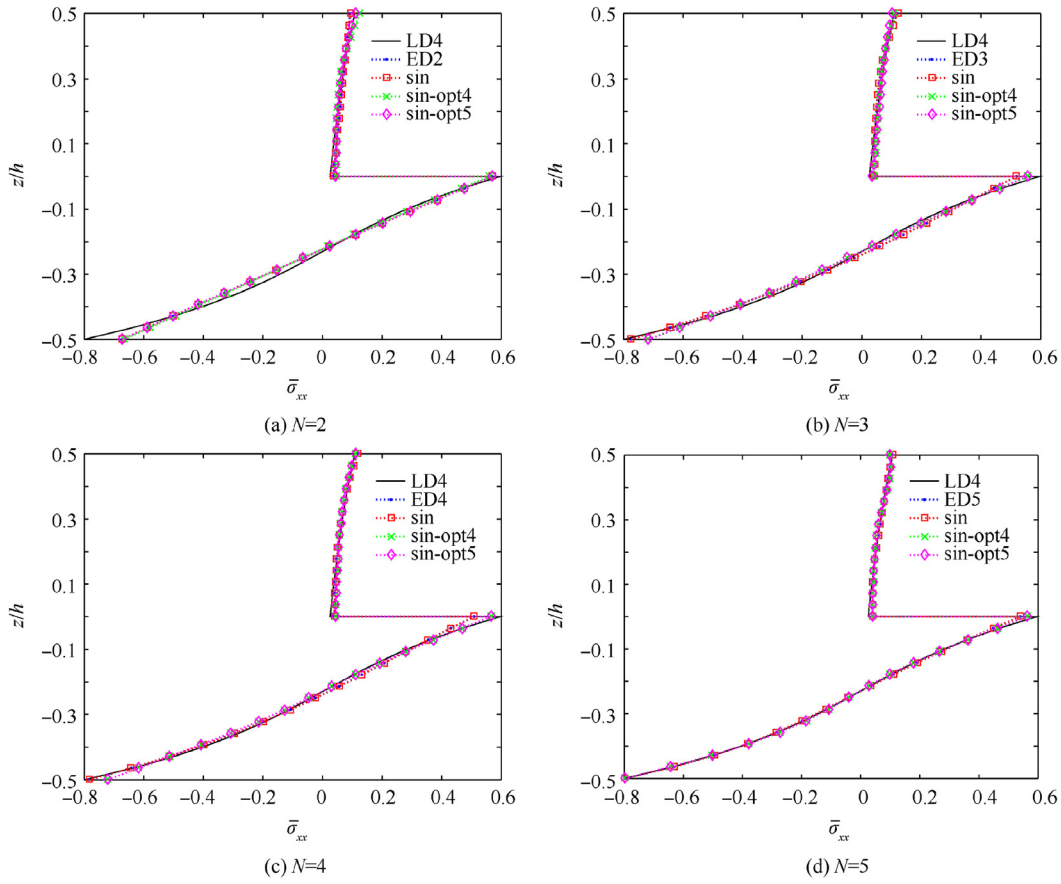

Fig. 6 Through-the-thickness distribution of dimensionless stress $\bar{\sigma}_{xx}$ for a (0°/90°) square laminated plate for sin displacement field and $N = 2, 3, 4, 5$.

integration in the thickness direction of the trigonometric expansion is not possible and the accuracy of this must necessarily be controlled. The formulation of the present stiffness nuclei was written in MATLAB and the integrations were obtained by quadrature function incorporated in MATLAB with 10^{-6} as tolerance.

3. Numerical results and discussion

Benchmark proposed by Demasi[43], which consists of two-layer asymmetric cross-ply simply supported plate (0°/90°), is utilized. Although the material properties do not have a practical use, the difficulty of this benchmark allows comparing several theories and evaluating different combinations of optimization parameters. A sinusoidal static load $q_z = \bar{Q}_z \sin(\alpha x)\sin(\beta y)$ applied at the top surface $(m = n = 1)$ of thick square plate $(a/h = 4, a = b)$ is considered in this paper. The mechanical properties of each layer are

Layer 1 (Bottom):

$$E_1 = 25E_2, E_3 = E_2, G_{23} = 0.2E_2, G_{12} = G_{13} = 0.5E_2, \upsilon = 0.25 \tag{29}$$

Layer 2 (Top):

$$E_1 = 25E_2, E_3 = 10E_2, G_{23} = 0.2E_2, G_{12} = G_{13} = 0.5E_2, \upsilon = 0.25 \tag{30}$$

The following non-dimensional quantities are used:

$$\begin{cases} \bar{w} = \frac{100E_2h^3}{\bar{Q}a^4} w\left(\frac{a}{2}, \frac{b}{2}, z\right) \\ \bar{\sigma}_{xx} = \frac{h^2}{\bar{Q}a^2} \sigma_{xx}\left(\frac{a}{2}, \frac{b}{2}, z\right) \\ \bar{\sigma}_{xz} = \frac{h}{\bar{Q}a} \sigma_{xz}\left(0, \frac{b}{2}, z\right) \end{cases} \tag{31}$$

Table 1 presents ED4 results obtained by using polynomial ESL theory of order 4 and layerwise (LW) theory LD4[56], and these results are compared with exact 3D solution provided in Ref.[43]. LD4 values present very close results for deflection $\bar{w}(z = h/4)$ and shear stress $\bar{\sigma}_{xz}(z = h/4)$ with errors equal to 0.005% and 0.106%, respectively. Furthermore, for normal stress $\bar{\sigma}_{zz}(z = h/4)$, the obtained error is 0.914%. In order to facilitate the calculation, LD4 was employed as reference result. In Table 1, ED4 and LD4 problem results are calculated by using classical form of Hook's law.

The percent error of deflection $\bar{w}(z = h/4)$, normal stress $\bar{\sigma}_{xx}(z = 0)$ and shear stress calculated by means of equilibrium equation $\bar{\sigma}_{xz}$ at $z = -h/4$ are obtained for several parameters r and s introduced in the trigonometric SSTFs (Eqs. (5) and (6)). The errors were computed using the following formula:

$$\text{err}R = \left|\left|1 - \frac{R}{R_{\text{LD4}}}\right|\right| \times 100\% \tag{32}$$

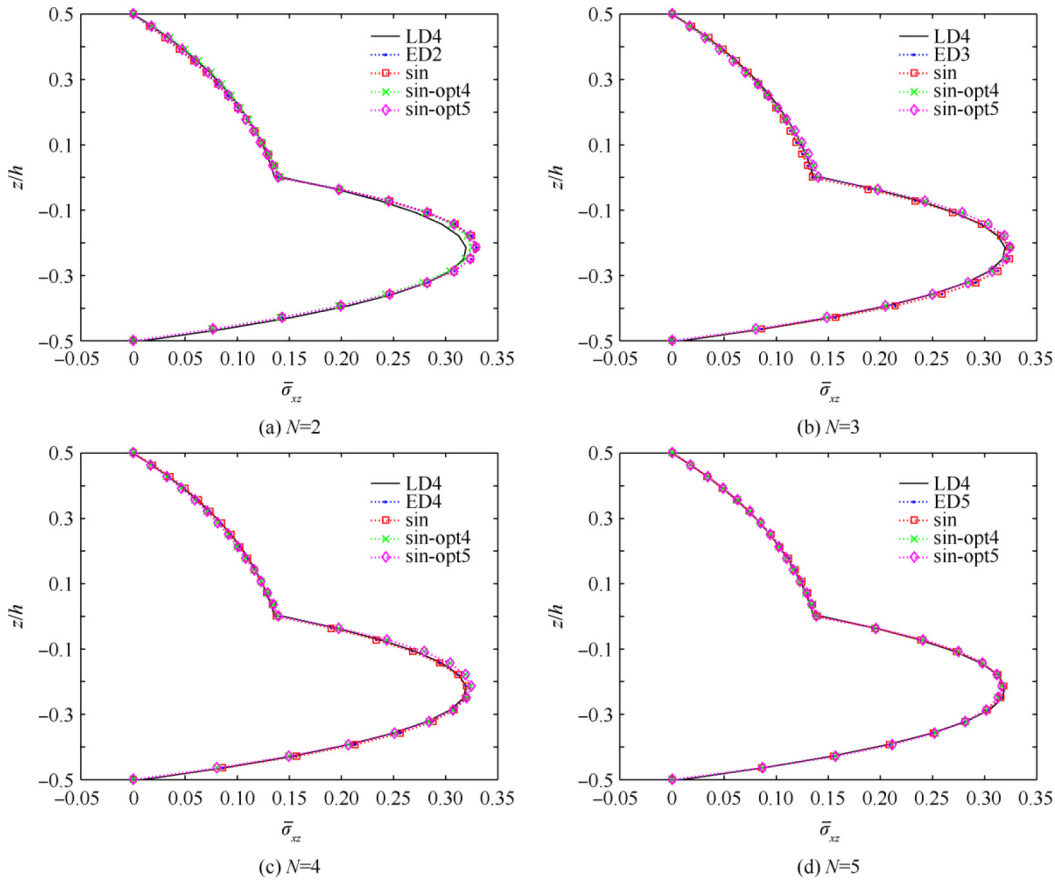

Fig. 7 Through-the-thickness distribution of dimensionless stress $\bar{\sigma}_{xz}$ for a (0°/90°) square laminated plate for sin displacement field and $N = 2, 3, 4, 5$.

where R refers to deflection or stress and R_{LD4} is the reference value obtained by LD4 theory. Additionally, average errors are given as

$$\mathrm{Av}X = \frac{w_1 \mathrm{err}\,\bar{w} + w_2 \mathrm{err}\bar{\sigma}_{xx} + w_3 \mathrm{err}\bar{\sigma}_{xz}}{w_1 + w_2 + w_3} \tag{33}$$

where w_i is arithmetic weights, i.e. deflection or stress values can be weighted (following a defined optimization criterion which needs to be further developed in future works) to impact or alleviate, depending on the case study, the average error and thus get the parameter of optimization (r, s). Five assumed optimization criteria are presented in Table 2 with their respective weight to calculate the average error ($\mathrm{Av}X$), so X adopt values from 1 to 5.

Parameters r and s were selected to get close to 3D solution of displacements and stresses, and in this way less percent error was produced according to weighted arithmetic means presented in Table 2. The weights depend on the relevance of the results to be evaluated. For example, normally, Av4 (equal weights) is chosen in the literature to calculate the average errors. Averages "Av1-Av3" represent independently the error of deflection $\bar{w}$, normal stress $\bar{\sigma}_{xx}$ and shear stress $\bar{\sigma}_{xz}$, respectively. Such criterion perhaps can be of interest in some applications where, for example, it is just relevant to knowing deflections. Additionally, an optimization criterion, with arbitrary weights to calculate the average error (Av5), is presented.

The variations of the average errors with the optimized parameters r and s considering an order of expansion of $N = 2$ and $N = 5$ for sin expansions are shown in Figs. 2 and 3, respectively. In the expansion $N = 2$, a great influence of the parameter s on the deflection $\bar{w}$ error (Av1) and average error (Av4) can be noticed. The low error values (blue zone) are for parameter s less than 5. The parameter r is important for the errors of the stresses $\bar{\sigma}_{xx}$ and $\bar{\sigma}_{xz}$ (Av2 and Av3). The areas with high errors (red zones) can be interpreted as incompatibility or instability of the SSTF. Fig. 3 shows low average error and a pronounced dependence on both optimized parameters. However, there are some instability areas with high percent error (see Av1 and Av2).

Figs. 4 and 5 show the variation of the various kinds of average error with the parameters r and s for sin$Z$ expansion when $N = 2$ and $N = 5$, respectively. In contrast to sin theory of order $N = 2$ (see Fig. 2), sinZ with order $N = 2$ presents pronounced dependence on both optimized parameters. Additionally, it shows several zones with low (blue) and high (red) average error. Although sinZ of order $N = 2$ presents lower percentage of errors than sin theory, the sinZ theory for $N = 2$ presents some instabilities produced perhaps for low performance of the SSTFs. On the other hand, the parameter s presents a great influence on the errors for sinZ expansion for the order $N = 5$ (see errors Av1 $(\mathrm{err}\,\bar{w})$, Av2 $(\mathrm{err}\bar{\sigma}_{xx})$ and Av4 (average error) in Fig. 5). Additionally, stability and low percent error are obtained for values of parameter s less than 6.

Optimized parameters are presented in Tables 3 and 4, where "sin-opt Y" (Y adopts values from 1 to 5) is the theory

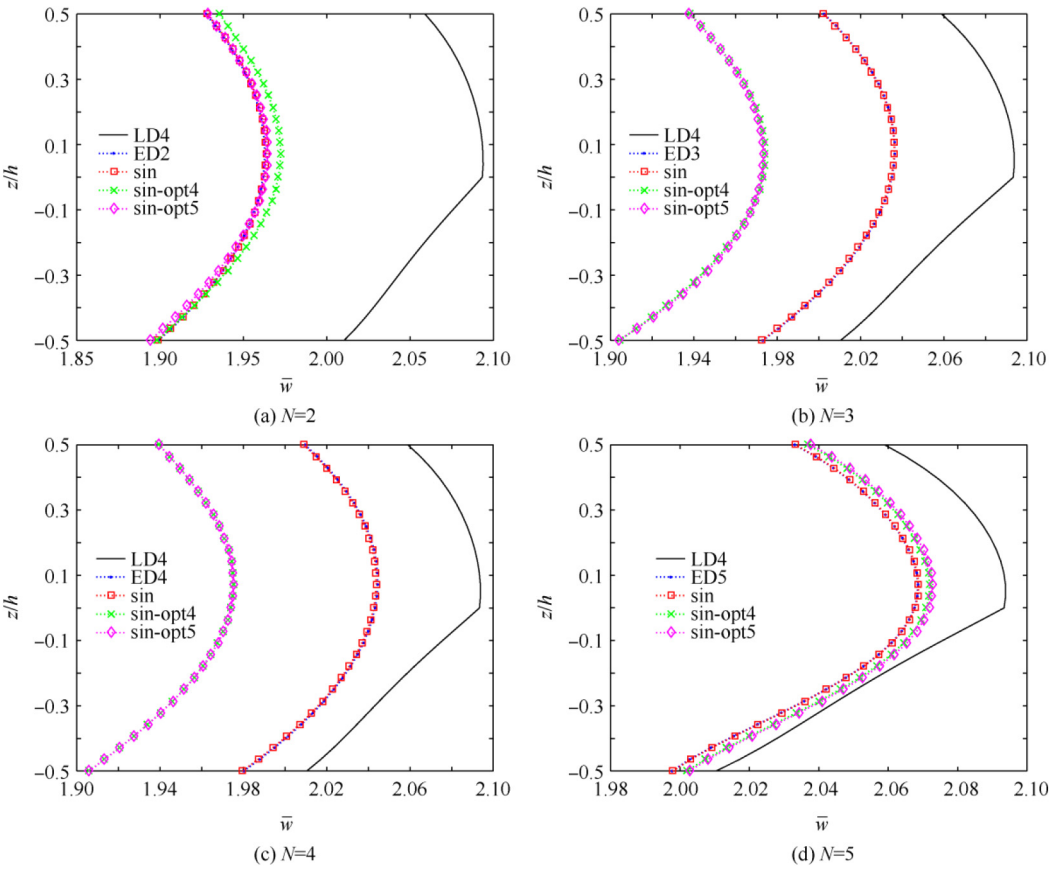

Fig. 8 Through-the-thickness distribution of dimensionless deflection $\bar{w}$ for a (0°/90°) square laminated plate for sin displacement field and $N = 2, 3, 4, 5$.

and the parameters are obtained by average error "AvX". In these tables, results of dimensionless deflection $\bar{w}(z = h/4)$, normal stress $\bar{\sigma}_{xx}(z = 0)$ and shear stress $\bar{\sigma}_{xz}(z = -h/4)$ are compared with LW theory by means of CUF (LD4)[34] for the side-to-thickness ratio $a/h = 4$. The errors in deflection (Av1) is lower for sin-opt1, but the average errors, such as Av4 or Av5, do not present significant improvement, as can be observed for $N = 2$. On the other hand, sin-opt4 and sin-opt5 present low percent of average error, but these reduce the precision in the deflection, as can be seen for $N = 3$ and 4. In Fig. 6, close values between LD4 and optimized trigonometric theory (opt4 and opt5), which overcome the Taylor and classical trigonometric displacement fields, are observed for $N = 3$ and 4 for normal stress $\bar{\sigma}_{xx}$ evaluated in $z = 0$ (bottom layer). The through-the-thickness distribution of shear stress $\bar{\sigma}_{xz}$, calculated by means of equilibrium equation, does not present better approximation than the classical trigonometrical expansion (without optimized parameter) (see Fig. 7). On the other hand, the through-the-thickness distribution of deflections $\bar{w}$ for opt4 and opt5, showed in Fig. 8, present a light improvement for $N = 2$ and 5, but these lose precision for $N = 3$ and 4. Fortunately, the idea is to select a model with reduced number of known variables.

Table 4 presents results for optimized trigonometric expansion with Zig-Zag model (sin$Z$-opt$X$) for different orders of expansion N compared with LD4 results. Moderate reduction of about 2% in the deflection error is obtained for sin$Z$-opt5 ($N = 2$) which is even less than Taylor and classical trigonometric expansion (without optimization); the reduction in average error (Av4) from approximately 5% to 1.8% can be achieved. Moreover, a considerable reduction in the Av4 from approximately 3.82% to 0.08% can be observed for $N = 3$. Nevertheless, for $N = 4$ and 5, very low reductions are achieved (up to 0.15%). The high number of SSTFs allows better accuracy in results, but these reduce the dependence on the optimization parameters r and s. Figs. 9–11 present the through-the-thickness distribution of normal stress $\bar{\sigma}_{xx}$, shear stress $\bar{\sigma}_{xz}$ and deflection $\bar{w}$. A good improvement with respect to non-optimization trigonometrical expansion (sin$Z$) is shown for the deflection $\bar{w}$ with sin$Z$-opt5 and sin$Z$-opt4 for $N = 2$ and 3. However, minimal improvement of the deflection is obtained for $N = 4$ and 5.

The practical application of this work relies on the optimization strategy to select a theory that best suits what is desired to achieve in a case problem, i.e. displacements, stresses or both. The method consists of incorporating (according to what is desired to get in terms of accuracy) several arithmetic weights in transverse displacements, normal stress and transverse shear stress. Consequently, a shear deformation theory that best suits with a particular experimental case problem can be persuaded. For example, one could be just interested in obtaining vertical deflection or good accuracy in terms of

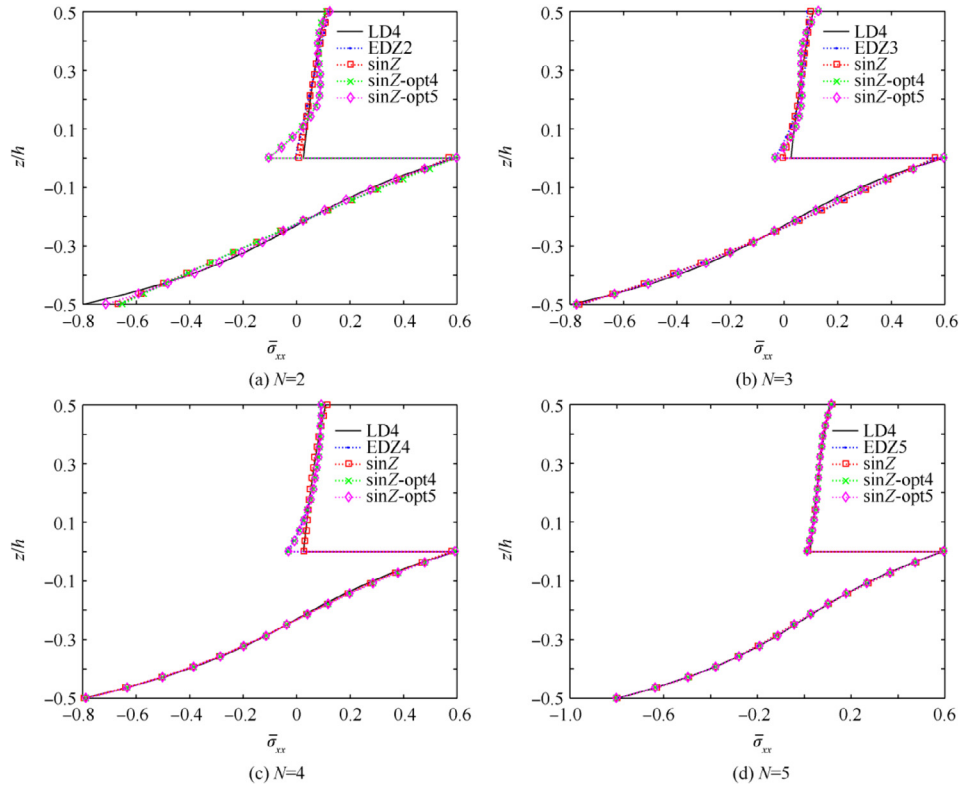

Fig. 9 Through-the-thickness distribution of dimensionless stress $\bar{\sigma}_{xx}$ for a (0°/90°) square laminated plate for sin$Z$ displacement field and $N = 2, 3, 4, 5$.

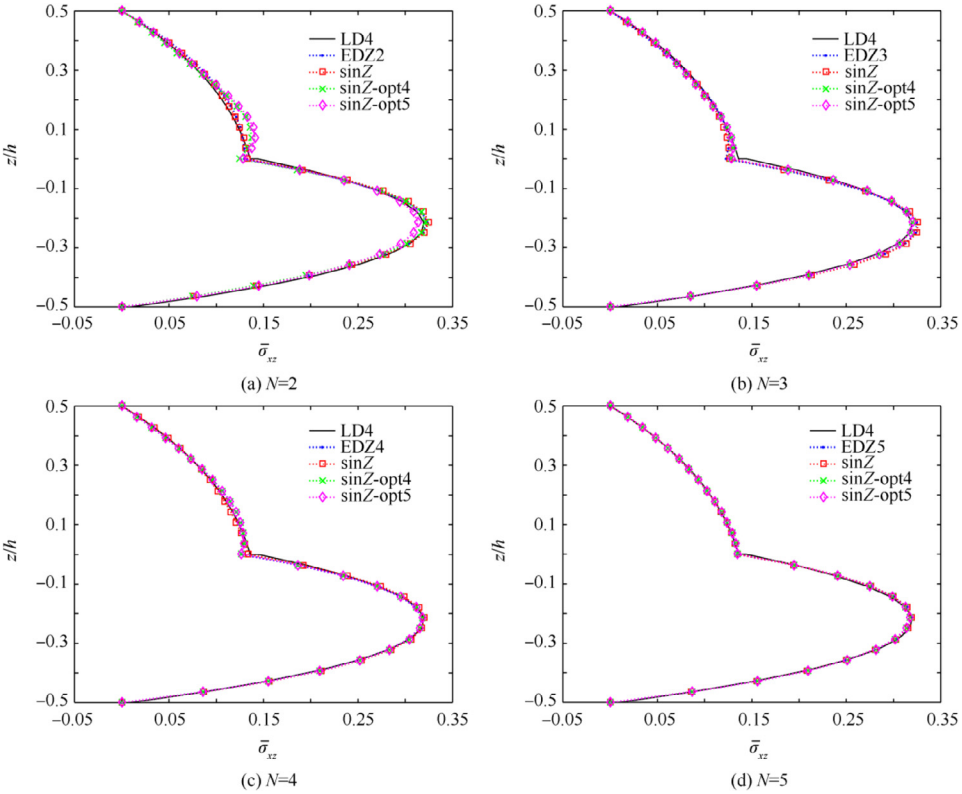

Fig. 10 Through-the-thickness distribution of dimensionless stress $\bar{\sigma}_{xz}$ for a (0°/90°) square laminated plate for sin$Z$ displacement field and $N = 2, 3, 4, 5$.

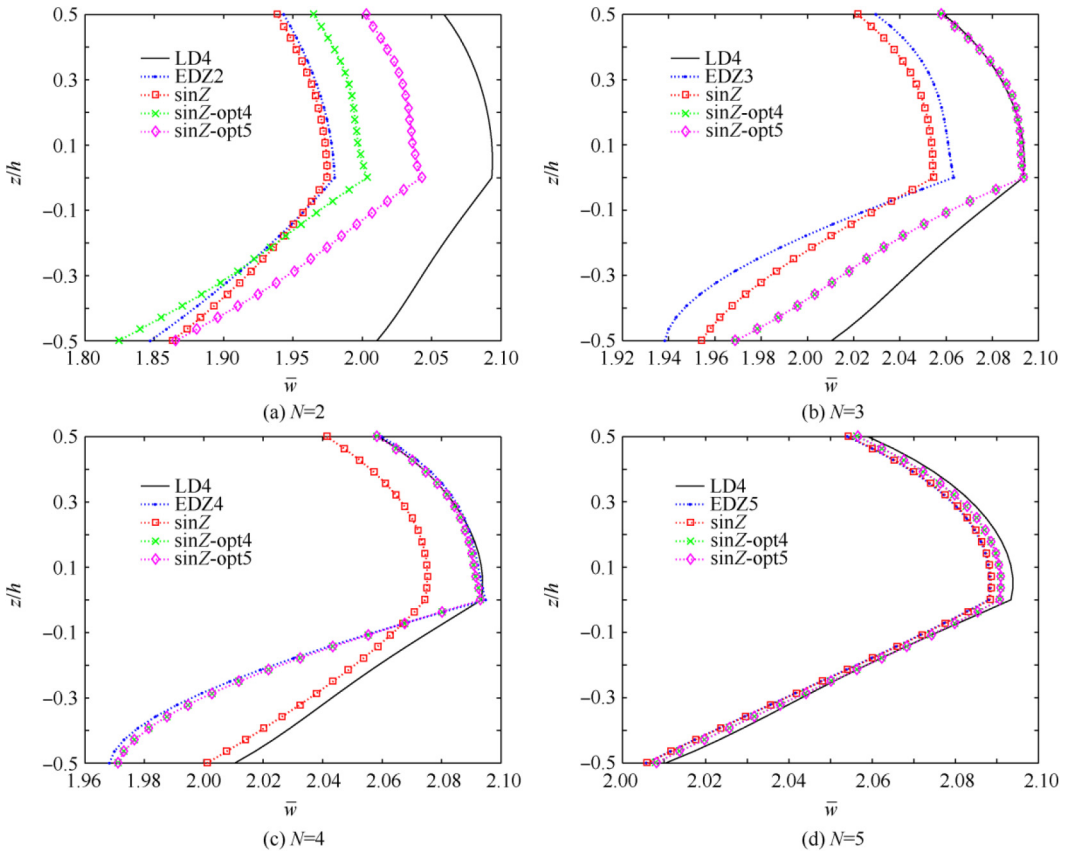

Fig. 11 Through-the-thickness distribution of dimensionless deflection $\bar{w}$ for a (0°/90°) square laminated plate for sin$Z$ displacement field and $N = 2, 3, 4, 5$.

shear stresses of advanced composite structures. This work can be a reference study to new numerical and experimental investigators by showing them that "case dependent problem" is a fact and so a shear deformation theory can be selected by weighting the desired output to best benefit the experiment validations through computational mechanics.

4. Conclusions

The present work introduces an optimized method in order to find reduced theories with better results than displacement field without optimization. Trigonometrical SSTFs with optimized parameters r and s contained in the in-plane and transverse displacements field are respectively developed by means of the CUF for analytical static problem of asymmetric laminated plate (0°/90°).

Governing equations are obtained by employing the PVD and are solved using Navier method solution. Several values and combination of optimization parameters are evaluated and selected by different criteria of average error.

A general displacement field was presented in this paper to use different displacement expansions, where $\boldsymbol{F}_\tau$, $\boldsymbol{G}_\tau$ and $\boldsymbol{H}_\tau$ are the SSTFs for the displacements in all the directions. In order to reduce the number of optimized parameters, trigonometrical displacement field with parameter r in $\times$ and y directions and parameter s in z direction are taken into account. Future studies are necessary in order to evaluate the influence of different non-polynomial SSTFs for the displacements in all the directions.

Improvement in the deflection and stress results for low order of expansions N are obtained by using an optimization procedure. However the optimization parameters depend on the plate geometry and the utilized order of expansion. Analytical axiomatic/asymptotic evaluation of the non-polynomial SSTFs needs to be performed to obtain reduced theories and evaluate the sensibility of the results by the variation of the optimized parameters r and s.

Acknowledgement

This paper was written in the context of the project: "Diseño y optimización de dispositivos de drenaje para pacientes con glaucoma mediante el uso de modelos computacionales de ojos" founded by Cienciactiva, CONCYTEC, under the contract number N° 008-2016-FONDECYT. The authors of this manuscript appreciate the financial support from the Peruvian Government.

References

1. Reissner E. The effect of transverse shear deformation on the bending of elastic plates. *J Appl Mech Trans ASME* 1945;**12**(2):69–77.
2. Mindlin RD. Influence of rotary inertia and shear on flexural motions of isotropic, elastic plates. *J Appl Mech Trans ASME* 1951;**18**(1):31–8.
3. Reddy JN, Liu CF. A higher-order shear of deformation theory of laminated elastic shells. *Int J Eng Sci* 1985;**23**(3):319–30.

4. Reddy JN. A simple higher-order theory for laminated composite plates. *J Appl Mech Trans ASME* 1984;**51**(4):745–52.
5. Levinson M. An accurate, simple theory of the statics and dynamics of elastic plates. *Mech Res Commun* 1980;**7**(6):343–50.
6. Librescu L. On the theory of anisotropic elastic shells and plates. *Int J Solids Struct* 1967;**3**(1):53–68.
7. Levy M. Memoire sur la theorie des plaques elastiques planes. *J Math Pures Appl* 1877;**30**:219–306.
8. Stein M. Nonlinear theory for plates and shells including the effects of transverse shearing. *AIAA J* 1986;**24**(9):1537–44.
9. Touratier M. An efficient standard plate theory. *Int J Eng Sci* 1991;**29**(8):901–16.
10. Soldatos KP. A transverse shear deformation theory for homogeneous monoclinic plates. *Acta Mech* 1992;**94**(3–4):195–220.
11. Karama M. Mechanical behavior or laminated composite beam by the new multilayer laminated composite structures model with transverse shear stress continuity. *Acta Mech* 2003;**40**:1525–46.
12. Mantari JL, Guedes Soares C. A trigonometric plate theory with 5-unknowns and stretching effect for advanced composite plates. *Compos Struct* 2014;**107**:396–405.
13. Zenkour AM. Generalized shear deformation theory for bending analysis of functionally graded plates. *Appl Math Modell* 2006;**30**(1):67–84.
14. Zenkour AM. Benchmark trigonometric and 3-D elasticity solutions for an exponentially graded rectangular plate. *Arch Appl Mech* 2007;**77**(4):197–214.
15. Zenkour AM. The effect of transverse shear and normal deformations on the thermomechanical bending of functionally graded sandwich plates. *Int J Appl Mech* 2009;**1**(4):667–707.
16. Zenkour AM. Hygro-thermo-mechanical effects on FGM plates resting on elastic foundations. *Compos Struct* 2010;**93**:234–8.
17. Mantari JL, Oktem AS, Guedes Soares C. Static and dynamic analysis of laminated composite and sandwich plates and shells by using a new higher order shear deformation theory. *Compos Struct* 2011;**94**:37–49.
18. Mantari JL, Oktem AS, Guedes Soares C. A new trigonometric deformation theory for isotropic, laminated composite and sandwich plates. *Int J Solids Struct* 2012;**49**:43–53.
19. Mantari JL, Granados EV, Guedes Soares C. Vibrational analysis of advanced composite plates resting on elastic foundation. *Compos Part B Eng* 2014;**66**:407–19.
20. Mantari JL, Bonilla EM, Guedes Soares C. A new tangential-exponential higher order shear deformation theory for advanced composite plates. *Compos Part B Eng* 2014;**60**:319–28.
21. Mantari JL, Guedes Soares C. Optimized sinusoidal higher order shear deformation theory for the analysis of functionally graded plates and shells. *Compos Part B Eng* 2014;**56**:126–36.
22. Houari MSA, Tounsi A, Bessaim A, Mahmoud SR. A new simple three-unknown sinusoidal shear deformation theory for functionally graded plates. *Steel Compos Struct* 2016;**22**(2):257–76.
23. Belabed Z, Houari MSA, Tounsi A, Mahmoud SR, Anwar Bég O. An efficient and simple higher order shear and normal deformation theory for functionally graded material (FGM) plates. *Compos Part B Eng* 2014;**60**:274–83.
24. Belkorissat I, Houari MSA, Tounsi A, Adda Bedia EA, Mahmoud SR. On vibration properties of functionally graded nano-plate using a new nonlocal refined four variable model. *Steel Compos Struct* 2015;**18**(4):1063–81.
25. Boukhari A, Atmane AH, Tounsi A, Adda Bedia EA, Mahmoud SR. An efficient shear deformation theory for wave propagation of functionally graded material plates. *Struct Eng and Mech* 2016;**57**(5):837–59.
26. Bennoun M, Houari MSA, Tounsi A. A novel five variable refined plate theory for vibration analysis of functionally graded sandwich plates. *Mech Adv Mater and Struct* 2016;**23**(4):423–31.
27. Bourada M, Kaci A, Houari MSA, Tounsi A. A new simple shear and normal deformations theory for functionally graded beams. *St and Compos Struct* 2015;**18**(2):409–23.
28. Mahi A, Adda Bedia EA, Tounsi A. A new hyperbolic shear deformation theory for bending and free vibration analysis of isotropic, functionally graded, sandwich and laminated composite plates. *Appl Math Model* 2015;**39**(9):2498–508.
29. Tounsi A, Houari MSA, Bessaim A. A new 3-unknowns non-polynomial plate theory for buckling and vibration of functionally graded sandwich plate. *Struct Eng Mech* 2016;**60**(4):547–65.
30. Ait Yahia S, Ait Atmane H, Houari MSA, Tounsi A. Wave propagation in functionally graded plates with porosities using various higher-order shear deformation plate theories. *Struct Eng Mech* 2015;**53**(6):1143–65.
31. Hebali H, Tounsi A, Houari MSA, Bessaim A, Adda Bedia EA. A new quasi-3D hyperbolic shear deformation theory for the static and free vibration analysis of functionally graded plates. *J Eng Mech ASCE* 2014;**140**:374–83.
32. El Meiche N, Tounsi A, Ziane N, Mechab I, Adda Bedia EA. A new hyperbolic shear deformation for buckling and vibration of functionally graded sandwich plates. *Int J Mech Sci* 2011;**50**(3):237–47.
33. Draiche K, Tounsi A, Hassan S. A refined theory with stretching effect for flexure analysis of laminated composite plates. *Geom and Eng* 2016;**11**(5):671–90.
34. Carrera E. Evaluation of layerwise mixed theories for laminated plate analysis. *AIAA J* 1998;**36**(5):830–9.
35. Carrera E. Developments, ideas, and evaluations based upon Reissner's mixed variational theorem in the modelling of multilayered plates and shells. *Appl Mech Rev* 2001;**54**(4):301–29.
36. Carrera E. Theories and finite elements for multilayered plates and shells: a unified compact formulation with numerical assessment and benchmarking. *Arch Comput Methods Eng* 2003;**10**(3):215–96.
37. Ferreira AJM, Carrera E, Cinefra M, Roque CMC, Polit O. Analysis of laminated shells by a sinusoidal shear deformation theory and radial basis functions collocation, accounting for through-the-thickness deformations. *Compos B Eng* 2011;**42**(5):1276–84.
38. Demasi L. ∞3 hierarchy plate theories for thick and thin composite plates: The generalized unified formulation. *Compos Struct* 2008;**84**:256–70.
39. Demasi L. ∞6 mixed plate theories based on the generalized unified formulation Part I: Governing equations. *Compos Struct* 2009;**87**:1–11.
40. Demasi L. ∞6 mixed plate theories based on the generalized unified formulation. Part II: Layerwise theories. *Compos Struct* 2009;**87**:12–22.
41. Demasi L. ∞^6 mixed plate theories based on the generalized unified formulation. Part III: Advanced mixed high order shear deformation theories. *Compos Struct* 2009;**87**:183–94.
42. Demasi L. ∞^6 mixed plate theories based on the generalized unified formulation. Part IV: Zig-zag theories. *Compos Struct* 2009;**87**:195–205.
43. Demasi L. ∞^6 mixed plate theories based on the generalized unified formulation. Part V: Results. *Compos Struct* 2009;**88**:1–16.
44. Filippi M, Petrolo M, Valvano S, Carrera E. Analysis of laminated composites and sandwich structures by trigonometric, exponential and miscellaneous polynomials and a MITC9 plate element. *Compos Struct* 2016;**150**:103–14.
45. Mantari JL, Ramos IA, Carrera E, Petrolo M. Static analysis of functionally graded plates using new non-polynomial displacement fields via Carrera Unified Formulation. *Compos Part B Eng* 2016;**89**:127–42.
46. Ramos IA, Mantari JL, Zenkour AM. Laminated composite plates subject to thermal load using trigonometrical theory based on Carrera Unified Formulation. *Compos Struct* 2016;**143**:324–35.
47. Miglioretti F, Carrera E, Petrolo M. Computations and evaluations of higher order theories for free vibration analysis of beams. *J Sound Vib* 2012;**331**(19):4269–84.

48. Carrera E, Miglioretti F, Petrolo M. Accuracy of refined finite elements for laminated plate analysis. *Compos Struct* 2010;**93**(5):1311–27.
49. Carrera E, Petrolo M. On the effectiveness of higher-order terms in refined beam theories. *J Appl Mech* 2011;**78**(2) 021013.
50. Carrera E, Petrolo M. Guidelines and recommendation to construct theories for metallic and composite plates. *AIAA J* 2010;**48**(12):2852–66.
51. Carrera E, Miglioretti F. Selection of appropriate multilayered plate theories by using a genetic like algorithm. *Compos Struct* 2012;**94**(3):1175–86.
52. Mantari JL. General recommendations to develop 4-unknowns quasi-3D HSDTs to study FGMs. *Aerosp Sci and Tech* 2016;**58**:559–70.
53. Mantari JL, Monge JC. Buckling, free vibration and bending analysis of functionally graded sandwich plates based on an optimized hyperbolic unified formulation. *Int J Mech Sci* 2016;**119**:170–86.
54. Vidal P, Polit O. A refined sinus plate finite element for laminated and sandwich structures under mechanical and thermomechanical loads. *Comput Methods Appl Mech Eng* 2013;**253**:396–412.
55. Carrera E, Filippi M, Zappino E. Laminated beam analysis by polynomial, trigonometric, exponential and zig-zag theories. *Eur J Mech – A/Solids* 2013;**41**:58–69.
56. Carrera E. Transverse normal stress effects in multilayered plates. *J Appl Mech* 1999;**66**(4):1004–12.